Wang, H. et al. (2013). Selenium-functionalized carbon as a support for platinum nanoparticles with improved electrochemical properties for the oxygen reduction reaction and CO tolerance. Journal of the Electrochemical Society, 160(4): 266 – 270.
http://dx.doi.org/10.1149/2.014306jes

Selenium-functionalized carbon as a support for platinum nanoparticles with improved electrochemical properties for the oxygen reduction reaction and CO tolerance

Hui Wang, Huahu Da, Shan Ji, Shijun Liao and Rongfang Wang

Abstract
Using selenium-functionalized carbon as supports, platinum nanoparticles were uniformly dispersed on the carbon surface, and showed improved electrochemical properties for the oxygen reduction reaction. At the same time the CO tolerance is improved. The method provides a new route for functionalization of the carbon surface on which to disperse noble metal nanoparticles for use as electrocatalysts in the oxygen reduction reaction.

Although great progress has been made in low-platinum and non-platinum electrocatalysts, Pt still dominates commerical electrocatalysts used in oxygen reduction reaction (ORR). Depositing Pt nanoparticles on a suitable support is an efficient way to reduce costs and improve performance.[1] The physicochemical properties of carbon supports have significant impact on the dispersion, stability and performance of Pt electrocatalysts.[2–5] Thus, many studies have been carried out to improve the properties of carbon supports.

It has been proven that the functionalization of carbon is an efficient way to improve the catalytic efficiency of a metal catalyst deposited on it.[6–8] Acid or base treatments to form functional groups including hydroxyls and carboxyls are the widely used methods to introduce the links, which can stabilize the interactions between catalyst and carbon supports.[9] Another way of functionalizing carbon is the doping of heteroatoms into carbon materials; this has attracted tremendous attention because of the improved physicochemical properties, such as high affinities to metals,[10] fast electron transfer rate and high thermal stability.[11] Among them, the doping of boron, phosphorus, nitrogen and sulfur to carbon supports have been proven to be beneficial to the activity and stability of Pt-based electrocatalysts.[10,12,13] Nevertheless, the above mentioned methods usually require rigorous conditions for several hours or days and are thus time consuming, which also make the procedures difficult to scale-up. Also, the treated carbon trends to be hydrophilic which creates filtration problems and often a decrease in conductivity.

Selenium, an element of the chalcogenide group, is a semi-metal with six of valence electrons, which could bond to the surface of carbon materials like sulfur. In addition,

selenium also has several advantages over the widely studied conventional heteroatom doping elements: 1) the electric conductivity of selenium is 20 orders of magnitude higher than that of sulfur, which facilitates electron transport during the electrochemical reactions;[14] 2) voltammetric studies show that suitably *t*-structured selenium is stable in acid solution and shows a double layer region from −0.2 to 0.75 V (vs. SHE), which is wider than that of Pt (~0.4 to ~0.7 V (vs. SHE));[15] 3) when selenium is bonded to metals, the catalyst may show better stability at high temperature due to the anchor effect;[16] 4) Selenium can become metallic when bound to Ru resulting in exceptional chemical stability of RuSe catalysts in acidic media due to the Ru → Se charge transfer, even at high positive potential.[17] To the best of our knowledge, selenium functionalized carbon as a support for electrocatalysts has not been reported before. Based on the above advantages, it is worthwhile to explore whether carbon can be functionalized with selenium as a support for highly active electrocatalysts toward ORR.

A simple strategy to dope selenium atoms on the surface of carbon by non-covalent functionalization depicted as Figure 1 was developed. Subsequently, Pt nanoparticles were then deposited on the surface of selenium-functionalized carbon (denoted as Pt/CSe_X), where the selenium atoms acted as a cross-linker between Pt particles and carbon. The electrochemical activity of the new catalyst was evaluated in terms of ORR by means of cyclic voltammetry (CV) and the CO tolerance of Pt/CSe_X was also compared with that of a conventional Pt/C catalyst. It was found that the activity and CO tolerance of this novel catalyst is significantly improved compared to that of conventional Pt/C.

Experimental

Carbon black (Vulcan XC-72R) was pretreated by washing in acetone, oxidizing in 2 mol L^{-1} HNO_3 and 30% H_2O_2, followed by washing with ultrapure water and drying overnight at 80°C, the pretreated carbon (denoted as C) was obtained. 0.185 g of triphenyl phosphine (PPh_3) was dissolved in 30 mL of tetrahydrofuran (THF) with stirring for 20 min, into which 0.0504 g elementary selenium was added and dissolved with stirring. 1 g of C was then dispersed ultrasonically into the THF solution containing Se and PPh_3 and transferred into a rotary dryer to evaporate the THF at 40°C. The mixture was dried in air at 60°C and thermally treated in a tubular furnace under N_2 atmosphere at 500°C for 2 h, and the obtained sample (denoted as CSe_X) was finally obtained.

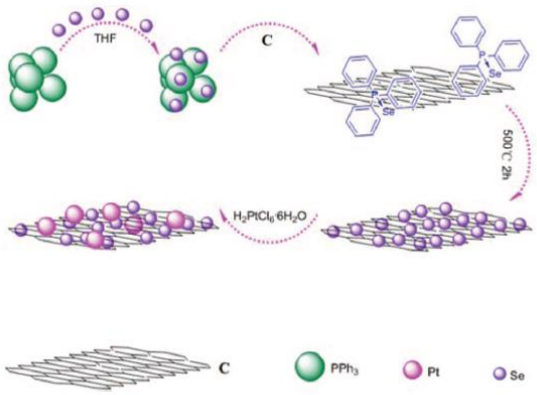

Figure 1. Diagram for selenium functionalized carbon and dispersion of Pt nanoparticles.

The catalyst was prepared by an organic colloid method in ethylene glycol solution. 3.32 mL of chloroplatinic acid (H_2PtCl_6 20 mg mL^{-1}) was dissolved in 30 mL of ethylene glycol and stirred for 20 min. The pH was adjusted to ~9 by adding 5 wt% KOH/ethylene glycol solution dropwise with vigorous stirring. 100 mg of CSe_X was then added into the flask and the mixture was sonicated for 20 min and stirred for 20 min to disperse the CSe_X. The temperature of the mixture was kept at 160°C for 6 h. The product was then filtered, washed with ultrapure water and dried at 60°C for 10 h. The Pt/CSe_X catalyst was obtained, and the metal loading was found to be about 20 wt%. For comparison, a Pt/C catalyst was also prepared by the same process.

The prepared materials were characterized by X-ray diffraction (XRD) using a Shimadzu XD-3A (Japan), with filtered Cu Kα radiation (40 kV, 40 mA). The Fourier-Transform infrared (FT-IR) spectra of KBr pellets were recorded in the 4000–400 cm^{-1} region on a Perkin-Elmer FT-IR M-1700 2B spectrophotometer. X-ray photoelectron spectroscopy (XPS) was carried out on a PHI-5702 multifunctional X-ray photoelectron spectrometer (American). Transmission electron microscopy (TEM) measurements were carried out on a JEM-2010 Electron Microscope (Japan) with an acceleration voltage of 200 kV. The chemical composition of the samples was determined by an IRIS advantage inductively coupled plasma atomic emission spectroscopy (ICP-AES) system (Thermo, America) and energy dispersive X-ray analysis (EDX) coupled to TEM.

The electrochemical measurements of catalysts were carried out on a CHI 650 electrochemical work station. A conventional three-electrode electrochemical cell was used for the measurements, including a platinum wire as the counter electrode, an Ag/AgCl (3 mol L^{-1} KCl) electrode as the reference electrode, and a rotating disk electrode (RDE, 5 mm in diameter) coated with the catalyst as the working electrode. All potentials presented are quoted with respect to the reversible hydrogen electrode (RHE), and current densities were normalized by the geometric area of the working electrode. The thin film electrode was prepared as follows: 5 mg of catalyst was dispersed ultrasonically in 1 mL of Nafion/ethanol (0.25 wt% Nafion). About 8 μL of the dispersion was transferred onto the glassy carbon

(GC) disk using a pipette, and then dried in the air for the preparation of the catalyst layer (40.8 μg_{Pt} cm^{-2} on the GC). Before each measurement, the solution was purged with high-purity N_2 and/or O_2 gas for at least 30 min to ensure the gas saturation. For the CO stripping voltammetry, CO gas was pre-adsorbed through the electrolyte of 0.5 mol L^{-1} H_2SO_4 solution for 10 min. The electrode was then placed in fresh 0.5 mol L^{-1} H_2SO_4 solution purged with a pure N_2 stream for 30min and cycled between 0.05 and 1.2 V versus RHE for two cycles at 50 mV s^{-1}. The currents are normalized to ECSA except the polarization curves for oxygen reduction reaction. All electrochemical measurements were carried out at room temperature.

Results and Discussion

The FT-IR spectra of C and CSe_X are plotted in Figure 2a. In the two curves, a broad band at ~3440 cm^{-1} is assigned to O–H stretching modes of OH group introduced upon treatment with H_2O_2, and those of carboxylic acid groups introduced by the treatment with HNO_3 are probably indicated by the C = O band at ~1640 cm^{-1}.[18] After selenium functionalized of carbon black, the band at ~1097 cm^{-1} located in the range of C–O stretching mode of ethers becomes apparent, which indicate a change in the CO dipole moment caused by the presence of selenium atoms.[7] The antisymmetric C–Se stretching at 605 cm^{-1}, the symmetric C–Se stretching at 507 cm^{-1} and the C–Se bending mode at 462 and 436 cm^{-1} cannot be clearly assigned in the FT-IR spectrum of CSe_X.[19] The results indicate possible non-covalent bonding of the selenium atoms. No characteristic diffraction peaks of PPh_3 are observed, implying that PPh_3 was removed by heat-treatment.

The XRD patterns (see Figure 3) of the two samples show coke-like structural features with disordered carbonaceous interlayers.[20] No peaks of elemental selenium were detected in the CSe_X sample which implies that the elemental selenium was present in atomic-layers dispersed on the carbon particles or in amorphous state. Furthermore, after the selenium functionalized C, there is no change in the position of the peaks, indicating that the selenium atoms were dispersed on the surface of C, but not incorporated into the carbon structure. On the other hand, the (100) and (004) peaks of the CSe_X sample, associated with crystalline carbon, are clearer than those of the C, suggesting that the CSe_X sample had a higher level of crystallinity.[21,22]

From the above results, it appears that the structure of carbon did not change after C was functionalized by selenium atoms. As further proof the morphology of the CSe_X sample, characterized by TEM shown in Figure 4. The original morphology of carbon shown as Figure 4a is a spherical form of a diameter of ca. 50 nm. After Se functionalized carbon, the morphology of carbon is consistent with the original morphology, and there are no obvious hetero-particles to be observed, suggesting Se atoms were dispersed on the surface of

carbon. The corresponding EDX spectrum of C and CSe_X inserted in Figure 4 indicates the presence of elemental selenium.

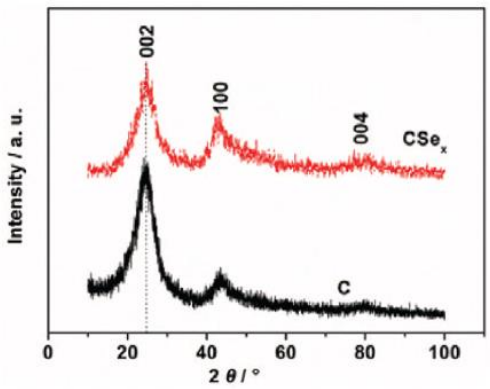

Figure 3. XRD patterns of CSex and C.

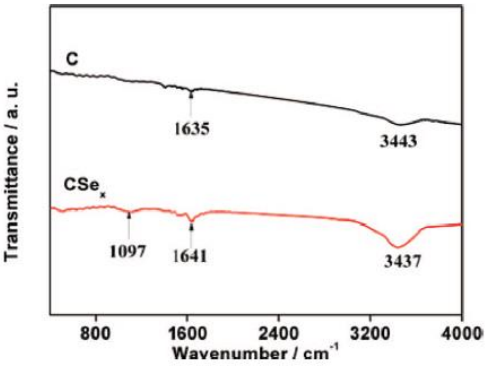

Figure 2. FT-IR spectra of C and CSe_x.

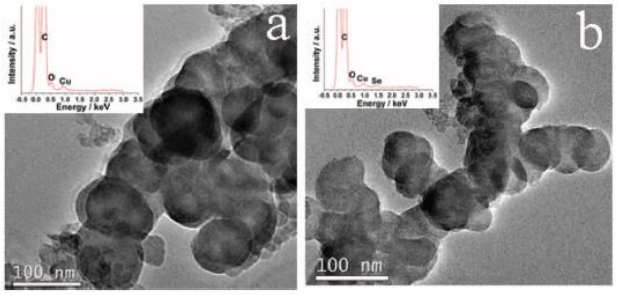

Figure 4. TEM images of C (a) and CSe_x (b) samples, respectively; Inset: the orresponding EDX spectra.

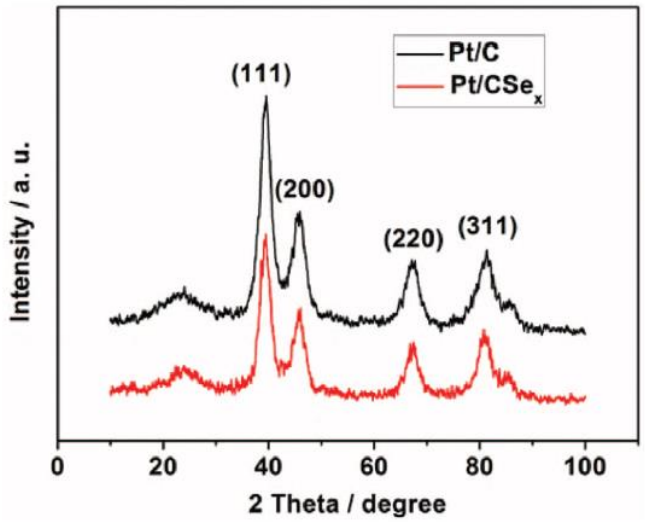

Figure 5. XRD patterns of the Pt/C and Pt/CSe$_x$ catalyst.

XRD patterns of Pt/CSe$_X$ and Pt/C catalysts are shown in Figure 5. The diffraction peak at about 25° in the two curves could be attributed to (002) plane of carbon. The Pt/C and Pt/CSe$_X$ catalysts display the (111), (200), (220) and (311) reflections of face-centered cubic Pt (JCPDS, No. 04-0802). This confirmed that the crystal structure of Pt nanoparticles is not affected by the presence of Se.

Figure 6 shows TEM images and the corresponding Pt particle size distribution of the Pt/CSe$_X$ and Pt/C catalysts. On the surface of CSe$_X$, Pt nanoparticles were well dispersed with diameters in the range of 2–6 nm (the inset of Fig. 6a), and no agglomeration was observed. Similarly, Pt nanoparticles were uniformly dispersed on the surface of C (see Fig. 6b), and the averge particle size and range of Pt nanoparticles supported on C compared to that on CSe$_X$ did not significantly enlarge from the inset of Fig. 6b. The practical composition of the Pt/CSe$_X$ catalyst was evaluated by ICP-AES analysis, which is about 19 wt% of Pt loading and 4 wt% of Se loading.

Figure 7 shows CVs of Pt/CSe$_X$ and Pt/C catalysts in N_2-saturated 0.5 mol L^{-1} H_2SO_4 solution, which normalized to geometric area of the electrode. The CVs exhibit hydrogen adsorption/desorption as well as oxide formation and reduction peaks, which are characteristic of a polycrystalline platinum electrode. For the Pt/CSe$_X$, The CV peak associated with oxide formation (0.8–0.9 V) becomes more pronounced relative to the Pt/C due to the contribution of the selenium oxidation.[23] On the other hand, the onset potential of oxide formation is shifted to more anodic potentials compared to that of the Pt/C, suggesting the delayed formation of Pt-oxides.[24]

The real surface of Pt catalysts could be estimated from the integrated charge of the hydrogen absorption region of the CV,[25] The evaluated electrochemical surface area are 48.3

and 43.5 $m^2\ g^{-1}_{Pt}$ for Pt/CSe_X and Pt/C catalysts, respectively, indicating that the electrochemical surface area of Pt/CSe_X catalyst is slightly larger than that of Pt/C catalyst.

Figure 8 shows RDE polarization curves of the Pt/CSe_X and Pt/C catalysts for oxygen reduction. It can be seen that the Pt/CSe_X catalyst had a higher half-wave potential, 43 mV more than that of the Pt/C catalysts. The kinetic current was calculated from the ORR polarization curve according to the Koutecky–Levich equation as follows:[26]

$$\frac{1}{i} = \frac{1}{i_k} + \frac{1}{i_d} \qquad [1]$$

where i is the experimentally measured current; i_d is the diffusion-limiting current, the diffusion control region was a high overpotential region lower than 0.6 V; and i_k is the kinetic current. Th n, the mass activity was calculated based on the following equation:

$$\text{mass activity} = \frac{i_k}{m} \qquad [2]$$

where m is the amount of Pt loading. The mass activities were calculated at 0.80 and 0.85 V versus RHE, which were shown as the inset in Fig. 8. The Pt mass activities of Pt/CSe_X

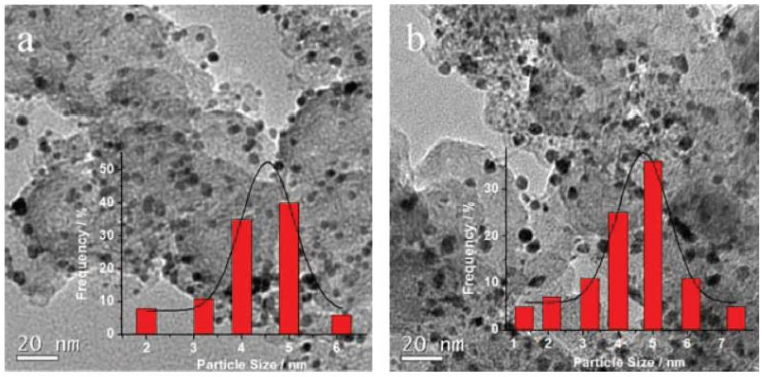

Figure 6. a) and b) TEM images of the Pt/CSe_x and Pt/C catalyst, respectively, Inset: the corresponding particle size distribution.

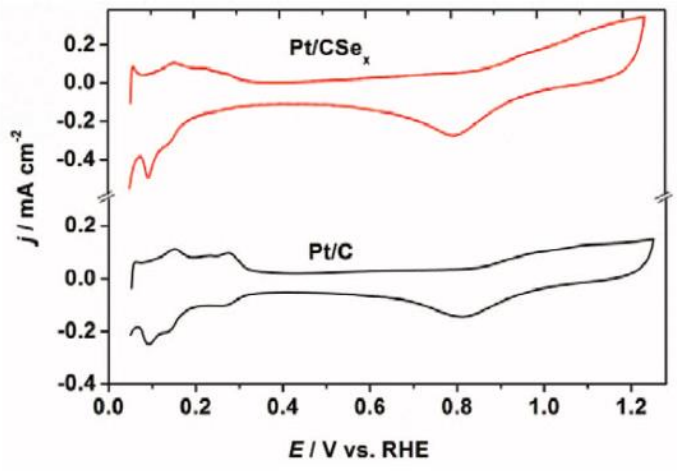

Figure 7. CVs of Pt/CSe$_x$ and Pt/C catalysts in N_2-saturated 0.5 mol L^{-1} H_2SO_4 solution, scanning rates: 50 mV s^{-1}.

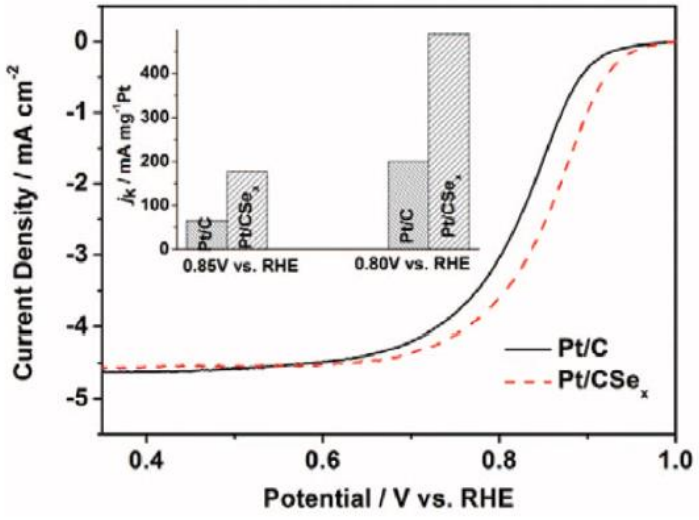

Figure 8. RDE polarization curves of Pt/CSe$_x$ and Pt/C catalysts for oxygen reduction, scanning rates: 5 mV s^{-1} and 1600 rpm; Inset: mass activity of Pt/CSe$_x$ and Pt/C catalysts at 0.80 and 0.85 V, respectively.

Table I. Binding energies and relative intensities of the Pt/CSex and Pt/C catalysts.

Samples	Species	Binding energies of Pt $4f_{7/2\ \&\ 5/2}$ [eV]	Relative intensities [%]
Pt/CSe$_x$	Pt(0)	70.98 & 74.20	57.5
	Pt(II)	72.01 & 75.21	32.8
	Pt(IV)	73.00 & 76.80	9.7
Pt/C	Pt(0)	70.87 & 74.20	46.5
	Pt(II)	71.67 & 75.09	38.0
	Pt(IV)	73.47 & 76.55	15.5

490.8 mA mg^{-1} at 0.85 and 0.80 V, which are 2.7 and 2.5 times as large as those of Pt/C (65.0 and 200.6 mA mg^{-1}), respectively.

The positive half-wave potential and higher mass activity of Pt/CSe_X indicate that the Pt/CSe_X catalyst has a higher ORR activity than the Pt/C catalyst. From the above discussion, the enhanced activity of the Pt/CSe_X catalyst is attributed to electric effect on Pt by the presence of Se.

In the d-band theory of Hammer and Nørskov,[27,28] it is claimed that the molecular adsorption energy is dependent primarily on the occupancy of the bonding and electronic structure of the valence band of the metal, especially its energy-weighted center, which can be well characterized by the position of the d-band center of a metal. The d-band center moving toward the E_F leads to a stronger chemisorption. Stamenkovic et al.[29] found that the ORR activity for Pt and Pt_3M (M = Ti, V, Fe, Co, and Ni) becomes higher with the d-band center moving away from E_F. Similar results were also reported by Lu group[30] and Lima group.[31] In line with this, the observed activity enhancement in this work is probably due to electronic factors on the Pt atoms caused by the contact with selenium atoms, which lead to the d-band center downshift, and moving away from the E_F will result in a weaker adsorption.

To illustrate the d-band center shift in the Pt/CSe_X catalyst, XPS analyzes of the prepared catalyst were performed (see Figure 9). Comparing the Pt binding energies, a positive shift in the Pt binding energies for Pt/CSe_X was observed. This shift of the doublet peaks to the higher binding energies can be attributed to d-band center downshifts, not the final state effect, because the final state effect is reported to emerge prominently for small clusters with a diameter less than 2 nm.[32] On the other hand, for the Pt/CSe_X catalyst, positive shifts demonstrated a stronger metal-support interaction than in the Pt/C catalyst. In addition, it was found that Pt contains various states, such as Pt(0), Pt(II) and Pt(IV), and that the ratios of the various Pt states displayed in Table I which were affected by the presence of selenium. Further evidence for d-band center downshift from CO stripping experiments was shown in Figure 10. The kinetic region of the ORR spread over the same potentials where the kinetics of the CO oxidation[30] also changed dramatically.

For the Pt/C catalyst, the peak potential was 870 mV, and the onset potential was 806 mV. For the Pt/CSe_X catalysts, a higher CO tolerance with a lower peak potential (852 mV) and onset potential (765 mV) compared to Pt/C was observed, due to the different effects of the carbon supports. The lower onset and peak potentials are considered to manifest better catalytic activity for CO oxidation, indicating a better CO tolerance for Pt/CSe_X.

In general, conventional elementary processes of the complete electrooxidation of CO are described in the following Figure 11. The CO adsorption energy is associated with the d-band

center. The Pt surface with a low d-band center value tends to bind adsorbents, i.e. CO, more weakly, which results in an increase the rate of step (2).[33]

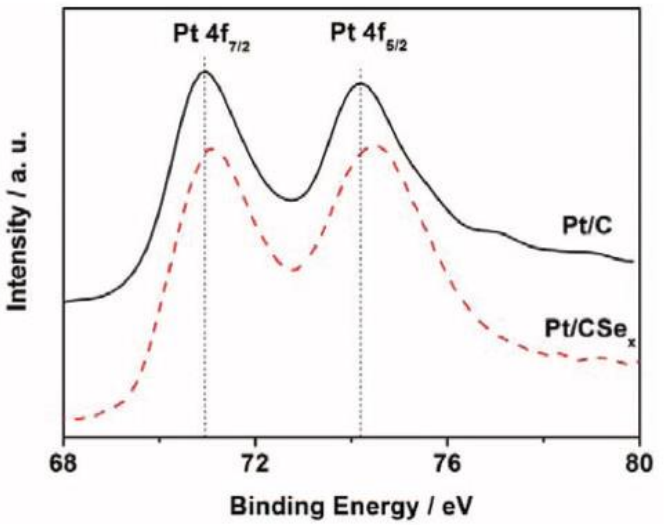

Figure 9. XPS spectra of Pt 4f bonds for the Pt/CSex and Pt/C catalysts.

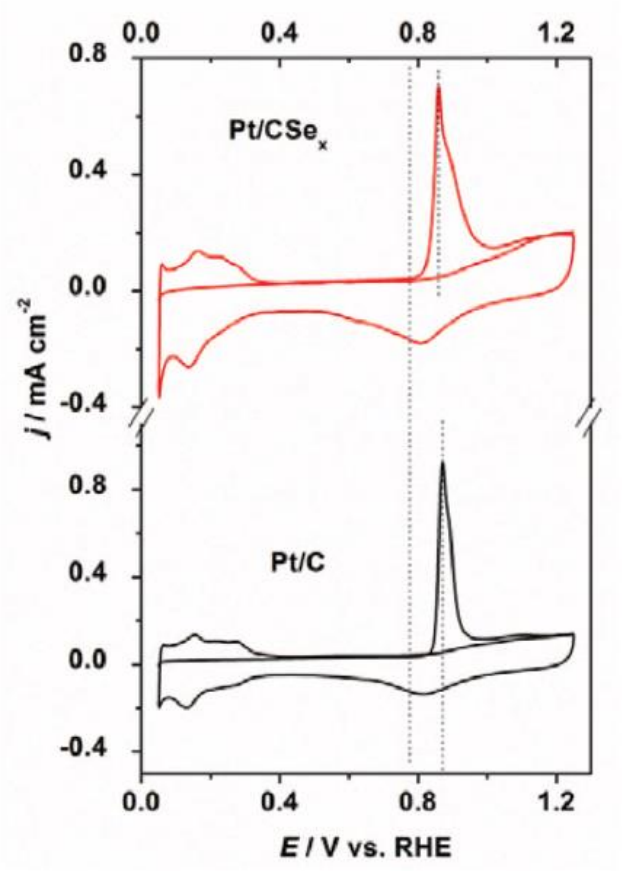

Figure 10. CO-stripping voltammetry for the Pt/CSe_x and Pt/C catalysts at 0.5 mol L^{-1} H_2SO_4 electrolyte, scanning rates: 50 mV s^{-1}.

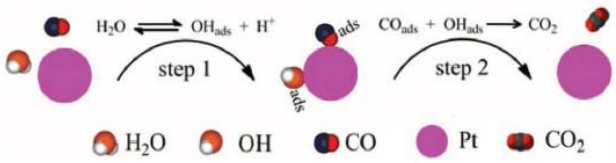

Figure 11. Diagram for the step of CO oxidation reaction on the surface of Pt nanoparticles.

On the surface of the Pt/CSe_X, the adsorption of CO became weaker, which leads to easier CO oxidation. Based on the above results, it can be concluded that the better catalytic activity for CO oxidation on Pt/CSe_X is promoted by electronic factors, e.g. the downshift of the d-band center.

Conclusions

A simple approach to functionalize the surface of carbon black using selenium elemental was demonstrated, and well-dispersed Pt nanoparticles with narrowly distributed particle size were formed on the surface of CSe_X. The electrochemical tests show that the Pt/CSe_X catalyst had a 2.7 times higher catalytic activity than that of the Pt/C catalyst in ORR. This enhanced electrochemical behavior most likely resulted from the d-band downshifts of Pt with the introduction of Se, and are demonstrated by the XPS and CO stripping measurements. This research strongly raises the possibility of using selenium as heteroatoms to functionalize carbon materials and replace the conventional carbon support for fuel cells. Furthermore, the improved CO tolerance of the Pt/CSe_X catalyst affords a new area of exploration in relation to poison durable catalysts for fuel cells.

Acknowledgments

The authors thank the National Natural Science Foundation of China (21163018), the National Science Foundation for Post-doctoral Scientists of China (20110490847, 2012T50554) and Guangdong Key Lab for Fuel Cell Technology for financially supporting this work.

References

1. Z. Liu, F. Su, X. Zhang, and S. W. Tay, *ACS Appl. Mater. Interf.*, **3**, 3824 (2011).
2. R. Yu, L. Chen, Q. Liu, J. Lin, K. L. Tan, S. C. Ng, H. S. O. Chan, G. Q. Xu, and T. S. A. Hor, *Chem. Mater.*, **10**, 718 (1998).
3. D. Pan, J. Chen, W. Tao, L. Nie, and S. Yao, *Langmuir*, **22**, 5872 (2006).
4. A. Guha, W. Lu, T. A. Zawodzinski Jr., and D. A. Schiraldi, *Carbon*, **45**, 1506 (2007).
5. W. Chen, Q. Xin, G. Sun, Q. Wang, Q. Mao, and H. Su, *J. Power Sources*, **180**, 199 (2008).
6. Z. B. Wang, G. P. Yin, and P. F. Shi, *Carbon*, **44**, 133 (2006).
7. C. Yang, X. Hu, D. Wang, C. Dai, L. Zhang, H. Jin, and S. Agathopoulos, *J. Power Sources*, **160**, 187 (2006).
8. S. Murugesan, K. Myers, and V. Subramanian, *Appl. Catal. B: Environmental*, **103**, 266 (2011).
9. H. Yoon, S. Ko, and J. Jang, *Chem. Commun.*, **43**, 1468 (2007).
10. K. Kwon, S. Jin, C. Pak, H. Chang, S. H. Joo, H. I. Lee, J. H. Kim, and J. M. Kim, *Catal. Today*, **164**, 186 (2011).
11. Y. Wan, X. Qian, N. Jia, Z. Wang, H. Li, and D. Zhao, *Chem. Mater.*, **20**, 1012 (2007).
12. Y. Zhou, R. Pasquarelli, T. Holme, J. Berry, D. Ginley, and R. O'Hayre, *J. Mater. Chem.*, **19**, 7830 (2009).
13. Y. Chen, J. Wang, H. Liu, R. Li, X. Sun, S. Ye, and S. Knights, *Electrochem. Commun.*, **11**, 2071 (2009).
14. A. Abouimrane, D. Dambournet, K. W. Chapman, P. J. Chupas, W. Weng, and K. Amine, *J. Am. Chem. Soc.*, **134**, 4505 (2012).
15. K. A. Kurak and A. B. Anderson, *J. Electrochem. Soc.*, **157**, B173 (2010).
16. Z. Wei, H. Guo, and Z. Tang, *J. Power Sources*, **62**, 233 (1996).
17. P. K. Babu, A. Lewera, J. H. Chung, R. Hunger, W. Jaegermann, N. Alonso-Vante,
    a. Wieckowski, and E. Oldfield, *J. Am. Chem. Soc.*, **129**, 15140 (2007).
18. S. Kim and S. J. Park, *J. Power Sources*, **159**, 42 (2006).
19. F. Cataldo, *Polyhedron*, **19**, 681 (2000).
20. M. Carmo, M. Linardi, and J. G. Rocha Poco, *Int. J. Hydrogen Energy*, **33**, 6289 (2008).
21. K. W. Park, Y. E. Sung, S. Han, Y. Yun, and T. Hyeon, *J. Phys. Chem. B*, **108**, 939 (2003).
22. G. Wu, L. Li, J. H. Li, and B. Q. Xu, *Carbon*, **43**, 2579 (2005).
23. L. Yan, Q. Jiang, D. Liu, Y. Zhong, F. Wen, X. Deng, Q. Zhong, B. Ren, and Z. Tian, *Acta Phys-Chim. Sinica*, **26**, 2337 (2010).
24. R. F. Wang, S. J. Liao, H. Y. Liu, and H. Meng, *J. Power Sources*, **171**, 471 (2007).
25. K. J. J. Mayrhofer, B. B. Blizanac, M. Arenz, V. R. Stamenkovic, P. N. Ross, and N. M. Markovic, *J. Phys. Chem. B*, **109**, 14433 (2005).
26. D. He, K. Cheng, H. Li, T. Peng, F. Xu, S. Mu, and M. Pan, *Langmuir*, **28**, 3979 (2012).
27. T. Bligaard and J. K. Nørskov, *Electrochim. Acta*, **52**, 5512 (2007).

28. B. Hammer, *Top. Catal.*, **37**, 3 (2006).
29. V. Stamenkovic, B. S. Mun, K. J. J. Mayrhofer, P. N. Ross, N. M. Markovic, J. Rossmeisl, J. Greeley, and J. K. Nørskov, *Angew. Chem. Int. Ed.*, **45**, 2897 (2006).
30. C. Lu, I. C. Lee, R. I. Masel, A. Wieckowski, and C. Rice, *J. Phys. Chem. A*, **106**, 3084 (2002).
31. F. H. B. Lima, J. Zhang, M. H. Shao, K. Sasaki, M. B. Vukmirovic, E. A. Ticianelli, and R. R. Adzic, *J. Phys. Chem. C*, **111**, 404 (2006).
32. E. Toyoda, R. Jinnouchi, T. Hatanaka, Y. Morimoto, K. Mitsuhara, A. Visikovskiy, and Y. Kido, *J. Phys. Chem. C*, **115**, 21236 (2011).
33. X. T. Zhang, H. Wang, J. L. Key, V. Linkov, S. Ji, X. L. Wang, Z. Q. Lei, and R. F. Wang, *J. Electrochem. Soc.*, **159**, B270 (2012).